Excess Hydrogen Bond at the Ice-Vapor Interface around 200 K

Wilbert J. Smit,[1,*] Fujie Tang,[2,3] M. Alejandra Sánchez,[3] Ellen H. G. Backus,[3] Limei Xu,[2,4] Taisuke Hasegawa,[3,5] Mischa Bonn,[3,†] Huib J. Bakker,[1,‡] and Yuki Nagata[3,§]

[1]*AMOLF, Science Park 104, 1098 XG Amsterdam, The Netherlands*

[2]*International Center for Quantum Materials, Peking University, 5 Yiheyuan Road, Haidian, Beijing 100871, China*

[3]*Max Planck Institute for Polymer Research, Ackermannweg 10, 55128 Mainz, Germany*

[4]*Collaborative Innovation Center of Quantum Matter, Beijing 100871, China*

[5]*Department of Chemistry, Graduate School of Science, Kyoto University, Sakyoku, Kyoto 606-8502, Japan*

(Received 13 March 2017; published 28 September 2017)

Phase-resolved sum-frequency generation measurements combined with molecular dynamics simulations are employed to study the effect of temperature on the molecular arrangement of water on the basal face of ice. The topmost monolayer, interrogated through its nonhydrogen-bonded, free O-H stretch peak, exhibits a maximum in surface H-bond density around 200 K. This maximum results from two competing effects: above 200 K, thermal fluctuations cause the breaking of H bonds; below 200 K, the formation of bulklike crystalline interfacial structures leads to H-bond breaking. Knowledge of the surface structure of ice is critical for understanding reactions occurring on ice surfaces and ice nucleation.

DOI: 10.1103/PhysRevLett.119.133003

Molecular-level details of water arrangement at the surface of ice are important for a variety of disciplines: for geology, the partial and transient melting of the grain boundaries of polycrystalline ice form the origin of the plastic flow of ice masses, leading to phenomena like glacier motion and frost heave [1]; for atmospheric science, the liquidlike layer on small ice particles constitute a medium for chemical reactions [2] and determines the interaction between ice particles; and for tribology, specifically on ice surfaces [3]. For all of these phenomena and processes, knowledge of the molecular structure of the outermost water monolayer, and how that structure changes with temperature is essential.

Experimentally, probing the ice surface entails two inherent challenges. The first is that the probe should be minimally invasive, since contacting the ice surface may cause melting and nonelastic deformation of the ice surface. This can occur in force measurements such as atomic force microscopy [4,5]. Optical methods are potentially less invasive but face a second challenge: to distinguish the response of the ice surface from the response of the bulk. This problem is frequently encountered using x rays [6,7] in studying the ice surface. Since the obtained signal from the ice sample contains both bulk and interfacial contributions, it is challenging to distinguish the interfacial contribution from the total signal in an unambiguous manner. Therefore, a technique with high surface-specificity would be of great advantage to study the molecular structure of the ice surface.

Sum-frequency generation (SFG) vibrational spectroscopy constitutes a noncontact and surface-specific measurement technique and therefore is ideal for exploring the ice surface. Vibrational SFG is a second-order nonlinear optical technique involving the generation of the sum frequency of infrared and visible pulses. This process is forbidden in centrosymmetric media. As such, the centrosymmetric bulk does not contribute to the signal, making SFG surface-specific [8,9]. In addition, when the infrared light is resonant with a vibrational transition, the SFG intensity will be resonantly enhanced, allowing for probing the vibrational modes of interfacial water molecules specifically.

Previously, the surface properties of ice have been studied with homodyne-detected SFG spectroscopy [10–17] as well as SFG simulations [13,18,19]. By measuring the SFG spectra of ice with different polarization combinations of infrared, visible, and sum-frequency lights, Shen and co-workers have shown that the ice surface becomes disordered above 200 K, while it appears ordered below 200 K [16,17]. Shultz and co-workers have studied the vibrational modes of hydrogen-bonded (H-bonded) O-H groups in the range of 3200 to 3600 cm^{-1} at the ice basal surface [10,12,14,15]. Nevertheless, the measured SFG response has not been clearly connected with the structural properties of the topmost ice surface layers. For example, although a simulation study has previously predicted the presence of excess H bonds at the ice—air interface [20], this has not yet been experimentally verified.

Here, we provide insight into the molecular arrangement of the topmost surface layers at the ice-air interface by combining MD simulations with phase-resolved SFG measurements in the temperature range of 150–245 K. We observe a rather gradual transition from a clear interfacial crystalline structure at low temperature, to a more disordered surface at higher temperatures. Both the low-temperature interfacial crystalline structure and the

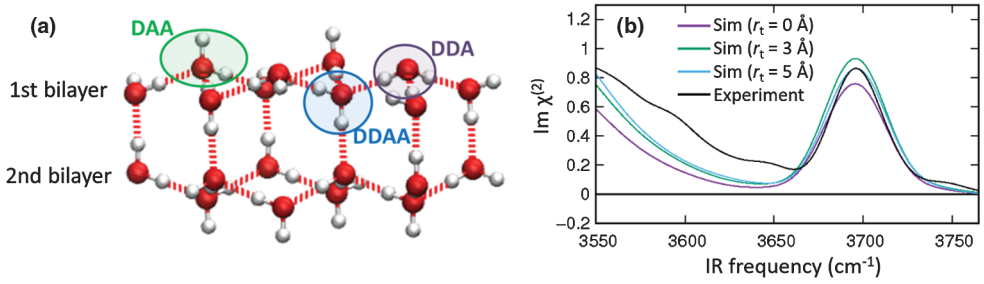

FIG. 1. (a) Schematic of the *DAA*, *DDA*, and *DDAA* water molecules at the basal ice-air interface with its perfect form. (b) Simulated SFG spectra in the free O-H region at 200 K with various cross-correlation cutoffs r_t along with the experimental result.

high-temperature structure are characterized by a reduced number of interfacial H bonds, but with very different conformations. As a result, increasing the temperature from below leads to a maximum in H-bonding density in the interfacial region around 200 K.

The preparation of single crystal ice and the experimental setup are detailed in our previous work [21]. In short, single crystalline ice was grown by seed extraction from the melt [13] and oriented between two crossed polarizers using a Rigsby stage [22]. A polished slice of 4 mm basal oriented ice was cut off and placed in a closed temperature cell which is cooled by liquid nitrogen. The SFG experiments in the O-H stretch vibrational region were performed in an *ssp*-polarization configuration indicating that the SFG and visible beams have a perpendicular polarization to the plane of incidence, while the infrared beam has a parallel polarization to the plane of incidence. Interference of the SFG signal originated at the ice surface with the SFG signal generated by a local oscillator (gold) allows for the determination of the phase-resolved *xxz* component of the second-order susceptibility $\chi^{(2)}$. The imaginary part of $\chi^{(2)}$ ($\mathrm{Im}\chi^{(2)}$) can be interpreted as a surface infrared absorption spectrum and is a sensitive probe of the molecular resonances at the ice-air surface.

Furthermore, we carried out MD simulations of the ice-air interface using a slab model. The simulation cell contains 1344 water molecules, forming 12 bilayers. Water molecules are modeled with the POLI2VS force field [23], which has been successful in simulating the SFG spectra of the liquid water-air interface [24–27]. The simulations were run in the canonical ensemble with the Nosé-Hoover thermostat. SFG spectra were generated by computing the time correlation function of the dipole moment and the polarizability [28] obtained from the POLI2VS MD trajectory. The time correlation functions were calculated by controlling the cross-correlation terms through the cutoff radius r_t within the truncated response function formalism [29]. This r_t sets the range over which the intermolecular couplings between water molecules are considered in the simulation. The relevant length scale for the intermolecular coupling is obtained when the spectrum no longer changes with increasing r_t. Details are provided in the Supplemental Material [30]. Note that SFG typically probes water molecules up to at most a few nm depth from the surface. However, here we focus on the SFG response of free O-H groups which are only present in the outermost molecular monolayer of the ice surface. As such, the spectroscopic probing depth is one monolayer in this study, but of course the spectral response of this outermost monolayer is influenced by the configuration of the deeper layers, e.g., surface reconstructions. The MD simulations account well for this influence.

Water molecules can be classified into three categories, based on the number of H bonds a water molecule donates (*D*) or accepts (*A*): *DAA* water molecules, i.e., water molecules donating one and accepting two H bonds, and, in the same notation, *DDA* and *DDAA* water molecules. These different types of water molecules are schematically depicted in Fig. 1(a). For the perfect form of the basal face, the topmost water monolayer consists of 50% *DAA* and 50% *DDA* water molecules [31]. Free O-H groups are associated solely with *DAA* molecules. However, in the range of 150–250 K, free O-H groups originate not only from *DAA* but also from *DA* water molecules with one donating and one accepting H bond. In the following, we will focus on the free O-H SFG response of the *DDA* and *DA* water molecules.

Figure 1(b) displays the simulated free O-H response at 3700 cm^{-1} at 200 K for different cutoff radii r_t together with the experimentally measured spectra. The simulated spectra are in good agreement with the experimental data. This figure further indicates that the SFG spectra simulated with $r_t = 0$, 3, and 5 Å are similar. This implies that the intermolecular vibrational coupling does not affect the free O-H stretch peak, justifying calculation of the SFG spectra with $r_t = 0$ Å to determine the temperature-dependent response.

The experimentally determined temperature dependence of the free O-H stretch $\mathrm{Im}\chi^{(2)}$ is shown in Fig. 2(a). Below 200 K, the peak position is invariant with temperature, while above 200 K it shifts to the blue with increasing temperature. These changes directly reflect a variation of the water structure at the ice interface. To understand the molecular origin of the 3700 cm^{-1} $\mathrm{Im}\chi^{(2)}$ feature at the ice-air interface in more detail, we computed SFG spectra at different temperatures with $r_t = 0$ Å. These are given in

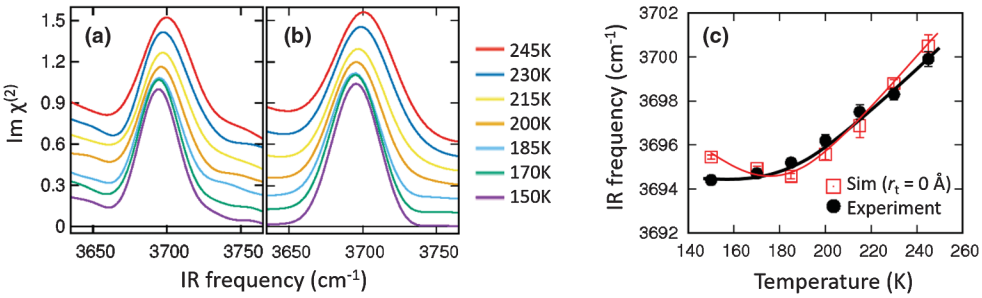

FIG. 2. Temperature dependence of (a) the experimentally measured free O-H stretch Im$\chi^{(2)}$ features; (b) the simulated Im$\chi^{(2)}$ features with $r_t = 0$ Å. The amplitudes of the peaks in the simulated spectra (b) are set to equal those in the experimental data (a). All spectra are offset by increments of 0.1 for clarity. (c) The free O-H stretch peak frequency vs temperature. The lines are to guide the eye. Error bars represent the 95% confidence intervals.

Fig. 2(b). Figure 2(c) summarizes the temperature dependence of the peak frequency in the experimentally measured and simulated SFG spectra. Both experiment and simulation data exhibit a rather similar increasing blueshift of the peak frequency with increasing temperature. The blueshift of the free O-H mode with increasing temperature is surprising, because for the liquid water-air interface the free O-H stretch mode redshifts when the temperature is increased, as is evident from MD simulations [26] and from heating effect observed in time-resolved SFG measurements [32]. A question arising here is why the peak frequency of the free O-H stretch mode of the ice-air interface is blueshifted with increasing temperature?

The blueshift of the free O-H stretch frequency may occur through the two following mechanisms. First, the free O-H frequency is affected by the frequency of the other O-H stretch mode within the same water molecule by intramolecular coupling [33]. It can be readily shown (see Supplemental Material [30]) that the change in intramolecular coupling from 150 to 245 K is responsible for at most a 1.2 cm^{-1} frequency shift, which is insufficient to account for the observed 6 cm^{-1} shift between 150 and

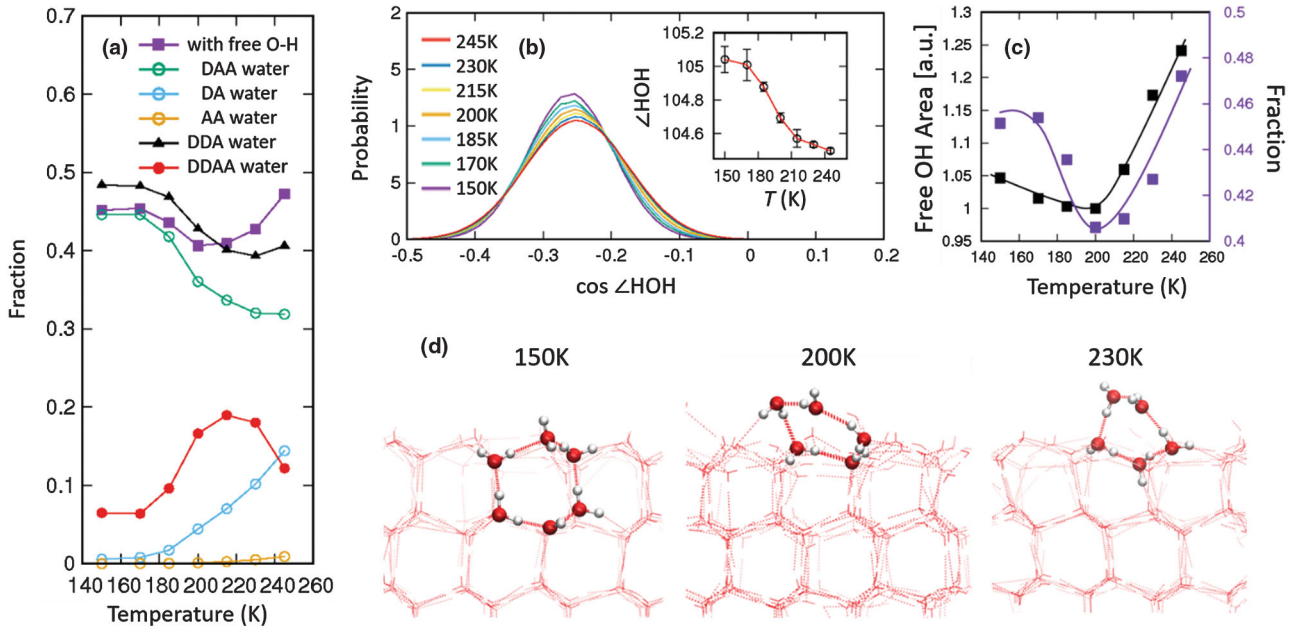

FIG. 3. (a) Simulated fraction of different interfacial water species (*DAA*, *DA*, *AA*, *DDA*, and *DDAA* water molecules) and total number of water molecules with free O-H groups (*DAA* + *DA* + *AA*) at the topmost monolayer of the ice surface. Error bars are smaller than the size of the symbols. (b) Variation of the intramolecular H-O-H angle of the DAA water molecules. The inset exhibits the H-O-H angle vs. temperature. Error bars represent 95% confidence intervals. (c) Temperature variation of the peak area of the experimentally measured free O-H SFG responses and the simulated fractions of water molecules with free O-H groups at the surface. (d) Schematics of the freezing process of ice for the basal surface of ice. This side view of the ice surface reveals that, with increasing temperature, the crystalline hexagonal structure present at 150 K starts to melt around 200 K; around this temperature the number of H-bonds is maximal, and the number of free O-H groups minimal.

245 K. Second, the free O-H frequency is determined by the number of H bonds accepted by the oxygen atom of the free O-H group [34,35]: Studies of small water clusters have revealed that the free O-H of a *DA* water molecule has a stretch frequency that is 20 cm^{-1} higher than for a *DAA* water molecule. Hence, a conversion of *DAA* to *DA*, with increasing temperature, would cause a blueshift of the free O-H stretch frequency.

To investigate whether a substantial conversion of *DAA* to *DA* occurs at the ice-air interface, we explored the interfacial composition of the water species vs temperature in the MD simulations. The result plotted in Fig. 3(a) shows that the fraction of the *DA* water molecules indeed increases dramatically with increasing temperature. Specifically, at 150 K, ~2% of the water molecules with free O-H groups ($DAA + DA + AA$ water molecules) consists of *DA* water molecules, while this fraction increases to ~30% at 245 K. Considering the frequency difference of ~20 cm^{-1} for the free O-H stretch modes of *DA* and *DAA* water molecules [34,35], a variation of the H-bond network of the water molecules with the free O-H groups indeed accounts for the observed 6 cm^{-1} shift of in the temperature-dependent SFG spectra.

Figure 3(a) reveals a second remarkable feature: up to ~200 K, the fraction of the *DAA* water molecules decreases with increasing temperature much faster than the fraction of the *DA* water increases. This means that with increasing temperature *DAA* water molecules are converted to *DDAA* water molecules, i.e., up to ~200 K, more hydrogen bonds are being formed, although the temperature is increasing.

To address the origin of this effect, we calculated the intramolecular H-O-H angle of the water molecules with the free O-H groups. Since the H-O-H angle increases by 2° when liquid water in the bulk is cooled down and converted to crystalline ice [36], it forms a good reporter for the local structure of crystalline ice. Figure 3(b) depicts the calculated temperature dependence of the H-O-H angle distribution of water molecules with free O-H groups, while the inset shows the average H-O-H angle of those water molecules vs temperature. The data illustrate that the change in H-O-H angle is accelerated below 200 K, indicating that below 200 K, the topmost ice surface increasingly starts to form a crystalline structure. When the temperature decreases below 200 K, *DDAA* water molecules in the deformed ring of the H-bond network break an H bond and form the crystal structure with the hexagonal H-bond network, thereby changing to *DAA* water molecules. As such, around 200 K, the number of free O-H groups is minimized and excess H bonds are generated, as is evident from the purple line of Fig. 3(a). The minimum number of the free O-H groups around 200 K is again fully consistent with the variation of the experimentally measured free O-H peak area, as shown in Fig. 3(c). Note that since the temperature variation of the simulated spectral area is critically affected by the quantum correction factor, a direct comparison with this area is rather arbitrary (see Supplemental Material [30]). The processes of the ice melting are summarized with the snapshots of the MD simulation in Fig. 3(d).

In summary, we have reported the temperature dependence of the free O-H SFG response of the ice Ih basal plane in both experiment and MD simulation. We show that the behavior reflects the temperature-dependent interconversion of differently hydrogen bonding-accepting and bond-donating water molecules at the ice surface. At elevated temperatures, thermal fluctuations cause breaking of hydrogen bonds; at low temperatures, the formation of crystalline interfacial structures also leads to an increase of free O-H groups at the surface. As a result, the topmost monolayer of ice has a minimum in free O-H groups and a maximum in hydrogen bonds around 200 K. These results are in particular important for understanding the dependency of the melting temperature to the size of the nanoscale ice [37] and clarify the surface-induced reorganization of the hexagonal ice to cubic ice [38] and proton ordering structure [31,39,40], as the stability of the interfacial ice structure governs the surface-induced melting and reorganization. Furthermore, the interconversion of *DAA* water to *DA* water affects the mobility of water [20]. The mobility of water governs the speed of nucleation and growth of ice [20,41–43] and is likely linked to the macroscopic properties of ice such as the friction of ice [3,44].

This work is financially supported by Max Planck Society. W. J. S. acknowledges the support from the research program of the Netherlands Organisation for Scientific Research (NWO). T. F. J. and X. L. M. acknowledge the support from NSFC (Grants No. 11290162, No. 11525520) and the National Key Research and Development Program of China (Grant No. 2016YFA0300901).

W. J. S. and F. T. contributed equally to this work.

Note added.—Recently, a heterodyne-detected SFG spectrum was measured at the ice-air interface [45].

*Present address: Laboratoire Sciences et Ingénierie de la Matière Molle, ESPCI Paris, PSL Research University, CNRS UMR 7615, 10 rue Vauquelin, 75005 Paris, France.
†bonn@mpip-mainz.mpg.de
‡bakker@amolf.nl
§nagata@mpip-mainz.mpg.de

[1] C. J. L. Wilson, Y. Zhang, and K. Stüwe, Cold Reg. Sci. Technol. **24**, 177 (1996).
[2] T. F. Kahan, J. P. Reid, and D. J. Donaldson, J. Phys. Chem. A **111**, 11006 (2007).
[3] A. M. Kietzig, S. G. Hatzikiriakos, and P. Englezos, J. Appl. Phys. **107**, 081101 (2010).
[4] H. Bluhm, T. Inoue, and M. Salmeron, Phys. Rev. B **61**, 7760 (2000).

[5] A. Döppenschmidt and H.-J. Butt, Langmuir **16**, 6709 (2000).
[6] H. Bluhm, D. F. R. a. N. K. Ogletree, C. Fadley, Z. Hussain, and M. Salmeron, J. Phys. Condens. Matter **14**, L227 (2002).
[7] A. Lied, H. Dosch, and J. H. Bilgram, Phys. Rev. Lett. **72**, 3554 (1994).
[8] Y. R. Shen and V. Ostroverkhov, Chem. Rev. **106**, 1140 (2006).
[9] M. Bonn, Y. Nagata, and E. H. G. Backus, Angew. Chem., Int. Ed. **54**, 5560 (2015).
[10] H. Groenzin, I. Li, V. Buch, and M. J. Shultz, J. Chem. Phys. **127**, 214502 (2007).
[11] V. Buch, T. L. Tarbuck, G. L. Richmond, H. Groenzin, I. Li, and M. J. Shultz, J. Chem. Phys. **127**, 204710 (2007).
[12] I. L. Barnett, H. Groenzin, and M. J. Shultz, J. Phys. Chem. A **115**, 6039 (2011).
[13] M. A. Sánchez, T. Kling, T. Ishiyama, M.-J. van Zadel, P. J. Bisson, M. Mezger, M. N. Jochum, J. D. Cyran, W. J. Smit, H. J. Bakker, M. J. Shultz, A. Morita, D. Donadio, Y. Nagata, M. Bonn, and E. H. G. Backus, Proc. Natl. Acad. Sci. U.S.A. **114**, 227 (2017).
[14] P. J. Bisson and M. J. Shultz, J. Phys. Chem. A **117**, 6116 (2013).
[15] H. Groenzin, I. Li, and M. J. Shultz, J. Chem. Phys. **128**, 214510 (2008).
[16] X. Wei, P. B. Miranda, and Y. R. Shen, Phys. Rev. Lett. **86**, 1554 (2001).
[17] X. Wei, P. B. Miranda, C. Zhang, and Y. R. Shen, Phys. Rev. B **66**, 085401 (2002).
[18] Q. Wan and G. Galli, Phys. Rev. Lett. **115**, 246404 (2015).
[19] T. Ishiyama, H. Takahashi, and A. Morita, J. Phys. Chem. Lett. **3**, 3001 (2012).
[20] G. J. Kroes, Surf. Sci. **275**, 365 (1992).
[21] W. J. Smit, F. Tang, Y. Nagata, M. A. Sánchez, T. Hasegawa, E. H. G. Backus, M. Bonn, and H. J. Bakker, J. Phys. Chem. Lett. **8**, 3656 (2017).
[22] H. W. Fairbairn and F. Chayes, *Structural Petrology of Deformed Rocks* (Addison-Wesley, Cambridge MA, 1954).
[23] T. Hasegawa and Y. Tanimura, J. Phys. Chem. B **115**, 5545 (2011).
[24] Y. Nagata, C.-S. Hsieh, T. Hasegawa, J. Voll, E. H. G. Backus, and M. Bonn, J. Phys. Chem. Lett. **4**, 1872 (2013).
[25] T. Ohto, K. Usui, T. Hasegawa, M. Bonn, and Y. Nagata, J. Chem. Phys. **143**, 124702 (2015).
[26] Y. Nagata, T. Hasegawa, E. H. G. Backus, K. Usui, S. Yoshimune, T. Ohto, and M. Bonn, Phys. Chem. Chem. Phys. **17**, 23559 (2015).
[27] J. Schaefer, E. H. G. Backus, Y. Nagata, and M. Bonn, J. Phys. Chem. Lett. **7**, 4591 (2016).
[28] A. Morita and J. T. Hynes, J. Phys. Chem. B **106**, 673 (2002).
[29] Y. Nagata and S. Mukamel, J. Am. Chem. Soc. **132**, 6434 (2010).
[30] See Supplemental Material at http://link.aps.org/supplemental/10.1103/PhysRevLett.119.133003 for Simulation protocols and supporting data including effects of intermolecular couplings and intramolecular couplings on frequency shift, calculation of frequency shifts of the free O-H stretch mode due to intramolecular vibrational couplings, discussion on consistency of our study with previous work, discussion on classical time correlation function and quantum correction factor, fraction of different interfacial water species with different H-bond definitions, and SFG spectra in the C-H stretch region.
[31] V. Buch, H. Groenzin, I. Li, M. J. Shultz, and E. Tosatti, Proc. Natl. Acad. Sci. U.S.A. **105**, 5969 (2008).
[32] K. Inoue, T. Ishiyama, S. Nihonyanagi, S. Yamaguchi, A. Morita, and T. Tahara, J. Phys. Chem. Lett. **7**, 1811 (2016).
[33] I. V. Stiopkin, C. Weeraman, P. A. Pieniazek, F. Y. Shalhout, J. L. Skinner, and A. V. Benderskii, Nature (London) **474**, 192 (2011).
[34] M. Fisher, J. P. Devlin, I. Ettischer, M. Melzer, V. Buch, J. Sadlej, J. Sadlej, V. Buch, T. Ebata, N. Mikami, and N. Haven, Science **304**, 1137 (2004).
[35] M. Miyazaki, A. Fujii, T. Ebata, and N. Mikami, Science **304**, 1134 (2004).
[36] G. S. Fanourgakis and S. S. Xantheas, J. Chem. Phys. **124**, 174504 (2006).
[37] D. Pan, L. Liu, B. Slater, A. Michaelides, and E. Wang, ACS Nano **5**, 4562 (2011).
[38] T. L. Malkin, B. J. Murray, C. G. Salzmann, V. Molinero, S. J. Pickering, and T. F. Whale, Phys. Chem. Chem. Phys. **17**, 60 (2015).
[39] D. Pan, L.-M. Liu, G. A. Tribello, B. Slater, A. Michaelides, and E. Wang, J. Phys. Condens. Matter **22**, 074209 (2010).
[40] T. Sugimoto, N. Aiga, Y. Otsuki, K. Watanabe, and Y. Matsumoto, Nat. Phys. **12**, 1063 (2016).
[41] O. Björneholm, M. H. Hansen, A. Hodgson, L. M. Liu, D. T. Limmer, A. Michaelides, P. Pedevilla, J. Rossmeisl, H. Shen, G. Tocci, E. Tyrode, M. M. Walz, J. Werner, and H. Bluhm, Chem. Rev. **116**, 7698 (2016).
[42] D. R. Haynes, N. J. Tro, and S. M. George, J. Phys. Chem. **96**, 8502 (1992).
[43] S. J. Cox, S. M. Kathmann, B. Slater, and A. Michaelides, J. Chem. Phys. **142**, 184704 (2015).
[44] A. S. de Wijn and L. G. M. Pettersson, Phys. Rev. B **95**, 165433 (2017).
[45] Y. Otsuki, T. Sugimoto, T. Ishiyama, A. Morita, K. Watanabe, and Y. Matsumoto, Phys. Rev. B **96**, 115405 (2017).

Supplementary Materials for:

Excess Hydrogen Bond at the Ice-Vapor Interface around 200 K

Wilbert J. Smit,[1,*,#] Fujie Tang,[2,3,#] M. Alejandra Sánchez,[2] Ellen H. G. Backus,[2] Limei Xu,[3,4] Taisuke Hasegawa,[2,5] Mischa Bonn,[2] Huib J. Bakker,[1] and Yuki Nagata[2]

1. AMOLF, Science Park 104, 1098 XG Amsterdam, The Netherlands

2. Max Planck Institute for Polymer Research, Ackermannweg 10, 55128 Mainz, Germany

3. International Center for Quantum Materials, Peking University, 5 Yiheyuan Road, Haidian, Beijing 100871, China

4. Collaborative Innovation Center of Quantum Matter, Beijing, China

5. Department of Chemistry, Graduate School of Science, Kyoto University, Sakyoku, Kyoto 606-8502, Japan

* Current address: Laboratoire Sciences et Ingénierie de la Matière Molle, ESPCI Paris, PSL Research University, CNRS UMR 7615, 10 rue Vauquelin, 75005 Paris, France

The authors contributed to this work equally

E-mail: nagata@mpip-mainz.mpg.de, bakker@amolf.nl, bonn@mpip-mainz.mpg.de

1 Simulation Protocols

1.1. Calculation of SFG Spectra

Since the method to obtain the SFG spectra from the simulation has been reported in Ref. [1,2], we describe the details briefly here. The resonant part of the SFG signal can be calculated with the truncating response function;

$$\chi_{xxz}^{\mathrm{res},(2)}(\omega; r_t) = iQ_{\mathrm{HC}}(\omega)\int_0^{\tau} \mathrm{d}t R_{xxz}^{(2)}(t; r_t) f(t) e^{-i\omega t}, \quad \text{(S1)}$$

where

$$Q_{\mathrm{HC}}(\omega) = \beta\hbar\omega/(1 - \exp(-\beta\hbar\omega)), \quad \text{(S2)}$$

is the harmonic quantum correction factor [3] and $\beta = 1/kT$. $f(t)$ is the Hann window function,

$$f(t) = \begin{cases} \cos^2(\pi t/2\tau), & 0 < t < \tau \\ 0, & t > \tau \end{cases}, \quad \text{(S3)}$$

where we used τ = 1.024 ps to compute the SFG spectra. The $\chi_{xxz}^{\mathrm{res},(2)}$ component corresponds to the SFG signal at the *ssp*-polarization configuration of the sum-frequency, visible, and infrared beams. Here, the *z*-axis forms the surface normal and the *xy*-plane forms the ice surface.

The truncating time correlation function $R_{xxz}^{(2)}(t; r_t)$ is given by

$$R_{xxz}^{(2)}(t; r_t) = \left\langle \sum_i g_{sc}^3(z_i(0))\mu_{zi}(0)\alpha_{xxi}(t) + \sum_i \sum_{j\neq i} g_{sc}(z_i(0)) g_{sc}^2(z_j(0))\mu_{zi}(0)\alpha_{xxj}(t) g_t(r_{ij}(0); r_t) \right\rangle, \quad \text{(S4)}$$

where μ_{ai} (t) ($\alpha_{abi}(t)$) is the a component of the molecular dipole moment (the ab component of the molecular polarizability) of water molecule i at time t. $g_t(r; r_t)$ is the function to determine the cross-correlation terms with the cross-correlation cutoff distance of r_t. The definition of $g_t(r; r_t)$ is

$$g_t(r; r_t) = \begin{cases} 1, & r \leq r_t \\ 0, & r > r_t \end{cases}, \quad \text{(S5)}$$

In order to avoid the cancellation of the molecular dipole moments at the two ice surfaces where the net orientations of water molecules at each surface are opposite, we multiplied the dipole moment by the screening function

$$\mathrm{g}_{sc}(z) = \mathrm{sign}\,(z) \times \begin{cases} 0, & |z| \leq z_{\mathrm{c1}} \\ \cos^2\left(\frac{\pi(|z|-z_{\mathrm{c2}})}{2(z_{\mathrm{c1}}-z_{\mathrm{c2}})}\right), & z_{\mathrm{c1}} < |z| \leq z_{\mathrm{c2}}, \\ 1, & z_{c2} < |z| \end{cases} \quad \text{(S6)}$$

where z is the z-coordinate of oxygen atom of a water molecule. Here, we set z_{c1} = 7 Å and z_{c2} = 8 Å, where the origin point of the z-coordinate was set to the center of mass of the system. The range of $z_{c1} < |z| < z_{c2}$ is located in-between two neighboring bilayers in the bulk (see Fig. S2).

The nuclear quantum effects lead to a red shift of the vibrational signatures of the SFG response of ice [4–6]. Since we did not include the nuclear quantum effects in the MD simulation, the resonant frequency was overestimated in the simulated SFG spectra. To compensate for this, the frequency was scaled down by a factor of 0.9592 to reproduce the experimentally obtained frequency of the free O-H stretch vibration. This

is slightly smaller than the scale factor of 0.96 we have used in the previous study for reproducing the entire O-H stretch frequency region [2,7–9].

1.2. Molecular Dynamics Simulation

We performed molecular dynamics (MD) simulations of the basal face of Ice (Ih) with the POLI2VS force field model [5]. The melting temperature of the POLI2VS model is 265 ± 5 K [8], in reasonable agreement with the experimental data. The simulation cell contained 1344 water molecules. Since the density of ice changes with temperature [10], we set the simulation cell size to 31.471382 Å × 31.14859 Å × 60 Å at 150 K, 31.488987 Å × 31.166015 Å × 60 Å at 170 K, 31.50459 Å × 31.181462 Å × 60 Å at 185 K, 31.52204 Å × 31.198735 Å × 60 Å at 200 K, 31.542267 Å × 31.21874853 Å × 60 Å at 215 K, 31.56196 Å × 31.238249 Å × 60 Å at 230 K, and 31.58424 Å × 31.26029 Å × 60 Å at 245 K. where 112 water molecules formed a basal face bilayer of ice. The system thus consisted of 12 bilayers.

In the force calculation, we used periodic boundary conditions for all *x*-, *y*-, and *z*-axes. The charge-charge, charge-dipole, and dipole-dipole interactions were calculated with the Ewald method, while the charge-quadrupole, dipole-quadrupole, quadrupole-quadrupole, and van der Waals interactions were smoothly truncated between 10 Å and 11.5 Å. The reversible reference system propagator algorithm method was employed to integrate the equations of motion [11]. A 0.2 fs time step was used to integrate the equations of motion for the intramolecular interactions with the sixth order symplectic

integrator [12], while a 0.4 fs time step was used for integrating the equations of motion for the intermolecular interactions with the second order symplectic integration scheme.

We prepared 25 randomly generated configurations of ice Ih with random proton ordering for 150, 170, 185, 200, 215, 230, and 245 K. The use of the random proton ordering for the SFG spectra calculation has been justified in Ref. [13], while the proton ordering of ice near the surface was predicted by Monte Carlo simulation [14]. We performed > 400 ps MD runs at 150, 170, 185, and 200 K, and > 250 ps MD runs at 215, 230, and 245 K in the *NVT* ensemble, where the system temperature was controlled by using the Nosé–Hoover chain thermostat [15]. Subsequently, we performed production MD runs under the same *NVT* condition. We obtained a total of 7.2, 7.5, 7.1, 10.7, 7.0, 7.5, and 7.9 ns-long MD trajectories for 150, 170, 185, 200, 215, 230, and 245 K, respectively. The analysis of the data of 200 K in Fig. 1(b) in the main text demonstrated that the SFG spectra simulated with r_t = 0 or 3 Å are well converged with ~5 ns MD trajectory, while the spectra with $r_t \geq 5$ Å needs ~10 ns MD trajectory. This means that we need more trajectories when r_t is large. This tendency is consistent with our previous work on the SFG spectra simulation at the water-air interface [7]. A snapshot of the ice structure at 200 K is shown in Fig. S1, while the density profile of water molecules is shown in Fig. S2.

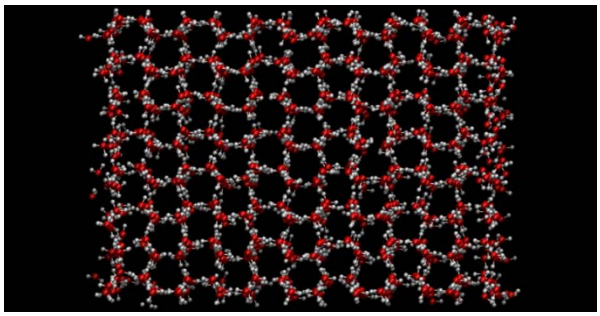

Figure S1. A snapshot of the simulated ice structure at 200 K. Note that our simulation has ~20 Å vacuum space separating the two ice surfaces.

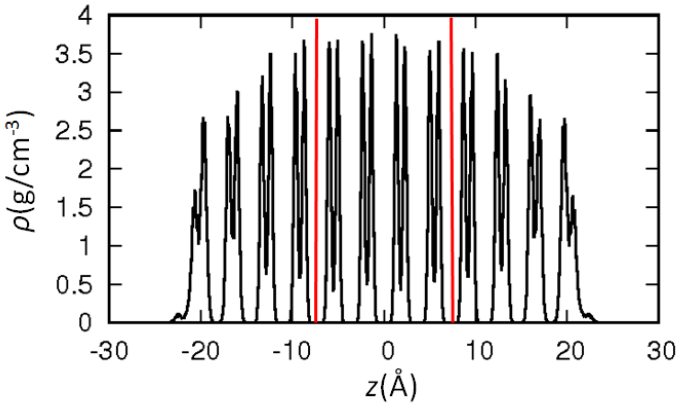

Figure S2. Density profile of the basal ice slab simulated at 200 K. The red lines represent $z = \pm z_{c2}$.

1.3. Definition of Hydrogen Bonded (H-Bonded) and Free O-H groups

Generating the sub-ensembles of water molecules, such as DA, DAA, DDA, and DDAA water molecules, depends on the H-bond definition, where 'D' denotes the water molecule has one donating H-bond and 'A' denotes the water molecule has one accepting H-bond. An important issue to connect these molecules with the free O-H peak in the SFG spectra is that the sub-ensemble of DA and DAA water molecules should reproduce the free O-H stretch peak and do not contain the O-H groups contributing to the lower frequency peaks. However, it is not clear whether the commonly accepted H-bond definitions [16–18] satisfy this condition. To check this, we calculated the contribution of the water molecules with the free O-H groups to the SFG spectrum by using one of the commonly accepted H-bond definition [17] and compared it with the free O-H stretch component. This free O-H stretch component was obtained through the fit using two Gaussians for the simulated SFG spectrum with r_t = 0 Å. The fit data are displayed in Fig. S3(a).

Subsequently, we calculated the contribution of the water molecules with the free O-H groups to the simulated SFG spectrum by using the H-bond definition given by Ref. [17]. Note that only the water molecules which had a free O-H group at time t = 0 were used in the calculation of the truncating time correlation function, Eq. (S4). The contribution of the water molecules with the free O-H groups is shown in Fig. S3(b). Apparently, the weakly H-bonded O-H group contributing to ~3600 cm^{-1} is contaminated in the contribution of the free O-H groups, when we used the H-bond definition of Ref. [17].

Therefore, we optimized the H-bond definition for capturing the sub-ensemble of the free O-H group. We optimized the criteria using the intermolecular O…O distance (R) and the angles formed by O-H…O (θ) in a similar manner to Ref. [19], giving the criteria of R < 4 Å and θ > 135°. The simulated contribution of the water molecules with the free O-H groups to the SFG spectrum is also shown in Fig. S3(b) as well. One can see that these criteria nicely reproduce the free O-H groups, while they reduce the amplitude of the 3600 cm^{-1} component, compared with the contribution of the free O-H group defined by the H-bond definition of Ref. [17]. As such, we used the criteria of R < 4 Å and θ > 135° for analyzing the contribution of the water molecules with the free O-H groups.

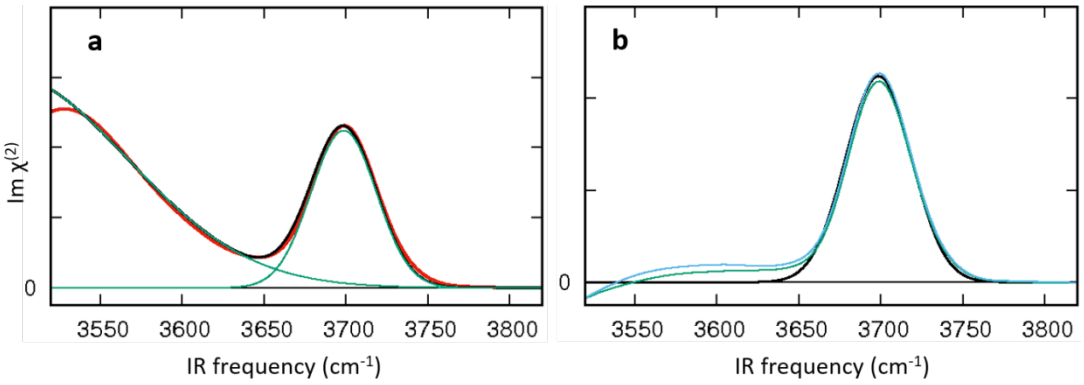

Figure S3. (a) Simulated SFG spectra with r_t = 0 Å (red) at 230 K, fitting data using two Gaussians in the frequency range of 3520 cm^{-1} < ω < 3820 cm^{-1} (black), and individual Gaussians (green). (b) Gaussian obtained from the fit (black) as well as simulated contribution of the water molecule with the free O-H groups calculated with the H-bond definition optimized here (green), and the definition given by Ref. 14 (blue).

2 Supporting Data

2.1. Effects of Intermolecular Couplings on Frequency Shift

In Fig. 1(b) of the main text, we compared the spectra of ice calculated with r_t = 0 and 3 Å at 200 K, from which we concluded that the intermolecular coupling of the free O-H stretch mode enhances the peak amplitude, but does not affect the peak positions. Since we discuss the tiny peak frequency variation of the free O-H stretch mode, we carefully check the effects of the intermolecular coupling on the frequency shift due to the temperature change. The temperature dependence of the peak frequency for the spectra calculated with r_t = 0 and 3 Å are plotted in Fig. S4.

Similar peak frequency shifts of the spectra calculated with r_t = 0 and 3 Å signify that the cross-correlation terms within the first hydration shell represented by r_t = 3 Å affect only the peak amplitude and does not shift the peak frequency. As such, hereafter, we consider the molecular origin of the frequency shift due to the temperature change in the SFG spectrum calculated with r_t = 0 Å.

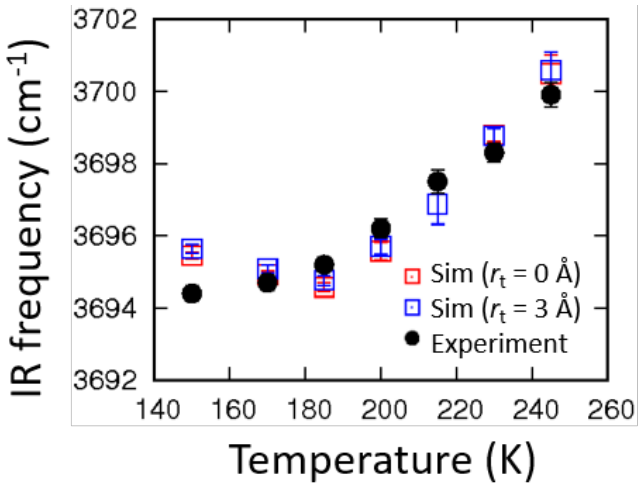

Figure S4. Peak frequency of the free O-H stretch vibration as a function of temperature. Red: Simulation with r_t = 0 Å, Blue: Simulation with r_t = 3 Å. Black: Experiment. Error bars represent the 95 % confidence interval.

2.2. Calculation of Frequency Shift of the Free O-H Stretch Mode due to Intramolecular Vibrational Couplings

The frequency of the free O-H stretch is influenced by intramolecular coupling with the H-bonded O-H group on the same H_2O molecule. When an uncoupled natural frequency of the free O-H stretch mode has frequency ω_{free} and the H-bonded O-H stretch mode has frequency ω_{HB}, these frequencies are shifted to $\omega_{free} + \Delta$ and $\omega_{HB} - \Delta$, respectively, due to intramolecular coupling. The frequency shift Δ is given by

$$\Delta \approx \gamma^2/(\omega_{free} - \omega_{HB}), \quad \text{(S7)}$$

where γ denotes the coupling strengths of the free O-H and H-bonded O-H stretch chromophores [20]. The coupling strength γ can be computed from ω_{free} and ω_{HB} through [21,22]

$$\gamma = \left(-1789 + 23852(E_{\text{free}} + E_{\text{HB}})\right)x_{\text{free}}x_{\text{HB}} - 1.966p_{\text{free}}p_{\text{HB}}, \quad \text{(S8)}$$

$$E_{\text{free/HB}} = \left(-2530 + \sqrt{2530^2 + 86225\left(3762 - \omega_{\text{free/HB}}\right)}\right)/86225, \quad \text{(S9)}$$

$$x_{\text{free/HB}} = 0.1934 - 1.75 \times 10^{-5}\omega_{\text{free/HB}}\ , \quad \text{(S10)}$$

$$p_{\text{free/HB}} = 1.611 + 5.893 \times 10^{-4}\omega_{\text{free/HB}}\ , \quad \text{(S11)}$$

where $\omega_{\text{free/HB}}$ has the unit of cm^{-1}. To calculate the distribution of the intramolecular coupling strength, we set ω_{free} = 3700 cm^{-1} and obtained the distribution of ω_{HB}, $P(\omega_{\text{HB}})$, (vibrational density of state for ω_{HB}) from the negative $\text{Im}\chi^{(2)}$ spectra contributed by the water molecules with free O-H group(s). The spectral shape of $\text{Im}\chi^{(2)}$ depends differs drastically from the density of state distribution due to the strong dependence of the transition dipole moment on the frequency, $\mu'(\omega)$ (solvation effects). The distribution of the density of states is obtained approximately by

$$P(\omega_{\text{HB}}) = \left|\text{Im}\chi^{(2)}(\omega_{\text{HB}})\right|/\mu'(\omega_{\text{HB}})\ . \quad \text{(S12)}$$

Note that since the transition polarizability is insensitive to the frequency, we omitted the frequency dependence of the transition polarizability in this formulation [22]. From these relations, we computed the distribution of the frequency shift Δ.

2.3. Effect of Intramolecular Coupling to Frequency Shift of Free O-H Group

We examined whether the vibrational frequency change of the H-bonded O-H stretch mode is sufficient for inducing the blue shift of 6 cm^{-1}, by evaluating the impact of the variation of the vibrational energy splitting due to temperature change on the frequency shift of free O-H groups. Since the calculation of the frequency shift due to the vibrational energy splitting (Δ) requires the frequency distribution of the other half H-bonded O-H groups, we calculated the SFG spectra contributed by the water molecules with the free O-H groups. This is plotted in Fig. S5(a). From the distribution of the H-bonded O-H stretch mode seen as a negative 3000 – 3500 cm^{-1} peak, we computed Δ in a similar manner to Ref. [20]. The frequency shift Δ due to the intramolecular coupling is plotted as a function of temperature in Fig. S5(b). The centers of mass for the frequency shifts are 1.67 cm^{-1} at 150 K and 2.90 cm^{-1} at 245 K, which difference of 1.2 cm^{-1} is insufficient to account for the observed frequency shift of 6 cm^{-1}. This means that the vibrational energy splitting is not a major contribution to induce the blueshift of the free O-H stretch frequency.

Here, we consider the reason why the frequency shift due to the intramolecular coupling is limited to 1.2 cm^{-1}. By comparing with liquid D_2O and D_2O-H_2O mixture water for which a shift of 17 cm^{-1} has been observed [20], this 1.2 cm^{-1} shift is very surprising. However, since the O-D stretch mode has lower frequency than the O-H stretch mode, the frequency difference of the free O-D and H-bonded O-D stretch modes is smaller than the frequency difference between the free O-H and H-bonded O-H stretch modes, making the energy splitting of these O-D stretch modes larger than that of the O-H

stretch modes. In fact, the frequency shift of the free O-H stretch between the neat H_2O and H_2O-D_2O mixture is ~10 cm^{-1} [23,24], smaller than that of 17 cm^{-1} for the O-D stretch case. Moreover, unlike the isotopic dilution where the H-bonded O-H frequency is ~ 1000 cm^{-1} higher than the H-bonded O-D stretch frequency, the temperature change from 150 K to 245 K induces the center frequency shifts of the H-bonded O-H stretch shift by ~100 cm^{-1}, as is clear from Fig. S5(a). As such, upon decreasing the temperature, the frequency shift of the free O-H stretch mode due to the intramolecular coupling is quite limited.

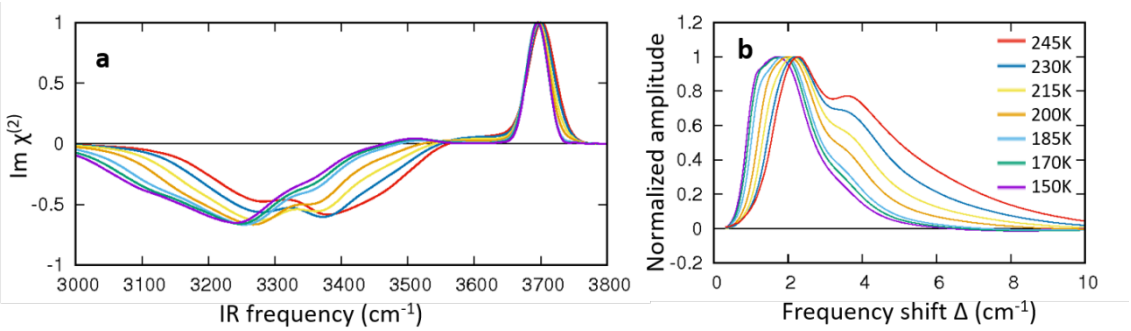

Figure S5: (a) Temperature dependences of the simulated SFG spectra contributed by the water molecules with the free O-H group. (b) Simulated temperature dependence of the frequency shift Δ due to the intramolecular coupling.

2.4. Consistency of Our Study with Previous Work

To examine whether our finding from the simulation is consistent with the previous SFG study by Shen and co-worker [25,26], where they claimed that the ordering of the topmost water monolayer is saturated at 200 K, we also calculated the angle, θ, of the O-H group of the water molecule with the free O-H group and the surface normal. This is shown in Fig. S6. The integrated probability, *P*, in the range of $-0.4 < \cos\theta < -0.2$ (inset of Fig. S6) indicates a steeper increase in *P* above 200 K than below 200 K. This is consistent with the data obtained by Shen and co-workers [25,26], but our data do not support the termination of the disordered structure at ~200 K. Rather, our finding points out that the ordered parameters obtained from the intensity data should be connected to the change in the number of DA water molecules. In fact, our data clearly illustrates that the topmost ice surface becomes hexagonally structured at temperatures below ~185 K.

Furthermore, we examined the consistency of the experimentally measured SFG data at the ice-air interface with the previous study. Figure S7 displays the comparison of the temperature dependence of the spectral frequency between the current study (2 data sets for our measurement) and Refs. [26]. These measurements show a consistent trend for the frequency shift of the free O-H peak.

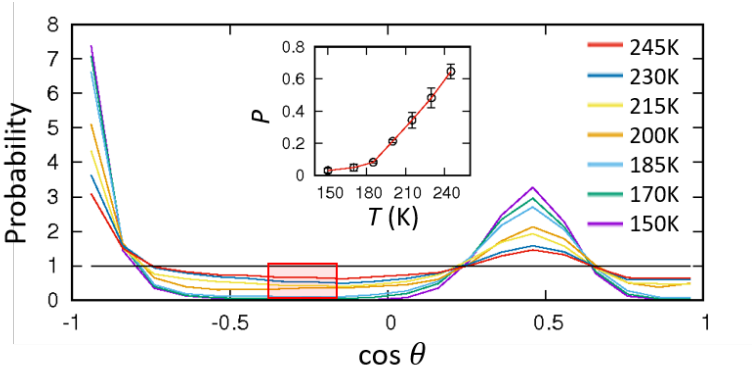

Figure S6. Distribution of angles θ formed by the O-H group of the water molecules with the free O-H group and the surface normal. The black line of unity probability represents random orientation. The inset shows the integrated probability, P, for $-0.4 < \cos\theta < -0.2$ (red-outlined region) vs. temperature. Error bars represent the 95 % confidence interval.

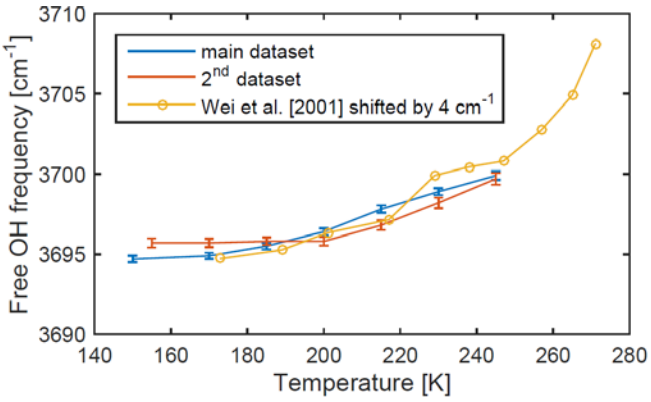

Figure S7. Peak frequency of the free O-H stretch vibration as a function of temperature. Two independent datasets used in our study (blue and red), the data from Ref. [26] (yellow) shifted by 4 cm^{-1} were plotted.

2.5. Classical Time Correlation Function and Quantum Correction Factor $Q(\omega)$

As is discussed in other works [27–29], the quantum correction factor is not uniquely defined and therefore many different forms of $Q(\omega)$ have been proposed. The choice of $Q(\omega)$ critically affects the temperature dependence of the amplitude of the vibrational spectra. Although it is believed that the harmonic quantum correction factor given in Eq. (S2) provides reasonable lineshapes and intensities of the infrared spectra of liquid water, [27,30–33] it is worth showing how the quantum correction factor has an effect on the frequency shift of the free O-H stretch peak. To examine it, we computed the variation of the SFG spectra with the harmonic correction factor (Eq. (S2)) and the standard correction factor

$$Q(\omega) = 2/(1+\exp(-\beta\hbar\omega)), \tag{S15}$$

as well as without quantum correction. These are plotted in Fig. S8.

The peak amplitude of the free O-H stretch mode vary substantially with the harmonic corrections factor (see Fig. S8(a)), while the standard correction factor and no correction factor does not enhance the peak amplitude (see Fig. S8(b) and (c), respectively.). Fig. S8(e) shows a comparison of the spectral area of the free O-H peak with the two quantum corrections. The standard correction factor does provide a local minimum around 200 K, but predicts a strong decrease in intensity at lower temperatures, not observed in the data with the harmonic correction factor. This may suggest that it may be too early to test the experimental SFG spectral area against the different theoretical corrections. In contrast, the frequency shift data is insensitive to the precise choice of the quantum correction factor (Fig. S8(d)).

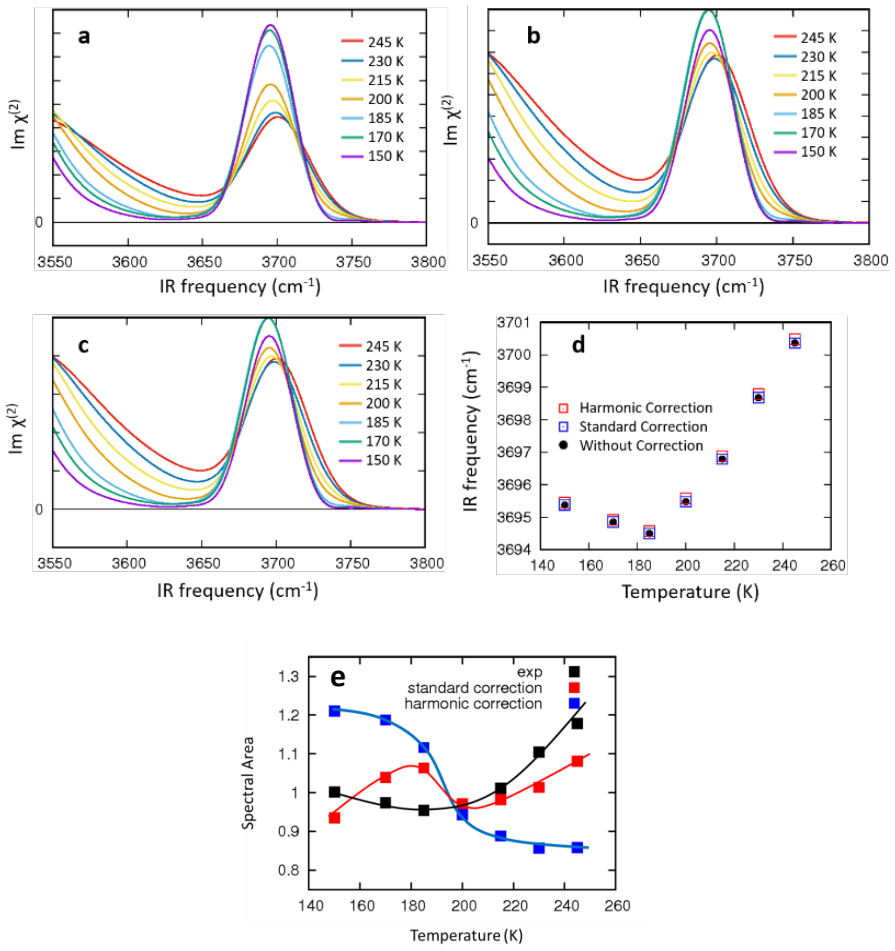

Figure S8. (a) Simulated SFG spectra with r_t = 0 Å for various temperatures based on a harmonic quantum correction. The normalized figures are given in Fig. 2(b) of the main text. (b) Simulated SFG spectra with r_t = 0 Å for various temperatures based on a standard quantum correction. (c) Simulated SFG spectra with r_t = 0 Å for various temperatures without quantum correction. (d) Peak frequency of the free O-H stretch vibration as a function of temperature, by using different quantum corrections. (e) Temperature variations of the spectral area with standard correction, harmonic correction, and without correction.

2.6. Fraction of Different Interfacial Water Species with Different H-Bond Definitions

In the main text, we have discussed the fraction of different interfacial water species (DAA, DA, AA, DDA, and DDAA water molecules) and total number of water molecules with free O-H groups (DAA + DA + AA) with the H-bonded/free O-H group definition defined in Section 1.3 of Supplementary Materials. We observed that the total number of water molecules with free O-H groups minimizes at around 200 K (see Fig. 3(a) in the main text).

To confirm that the observed minimum in free O-H groups does not depend on the explicit H-bonded/free O-H group definition, we also calculated the fractions of the water species using another H-bond definition. We used a H-bond criteria of R < 3.5 Å and β < 50°, where β denotes the H-O…O angle. [34] This was known to provide a good free O-H definition. The calculated fraction data are shown in Fig. S9. Similar to the calculations presented in the main manuscript (Fig. 3(a)), the fraction of water molecules with the free O-H groups shows a minimum around 200 K, demonstrating that the observed maximum in surface H-bond density around 200 K is insensitive to the H-bonded/free O-H group definition.

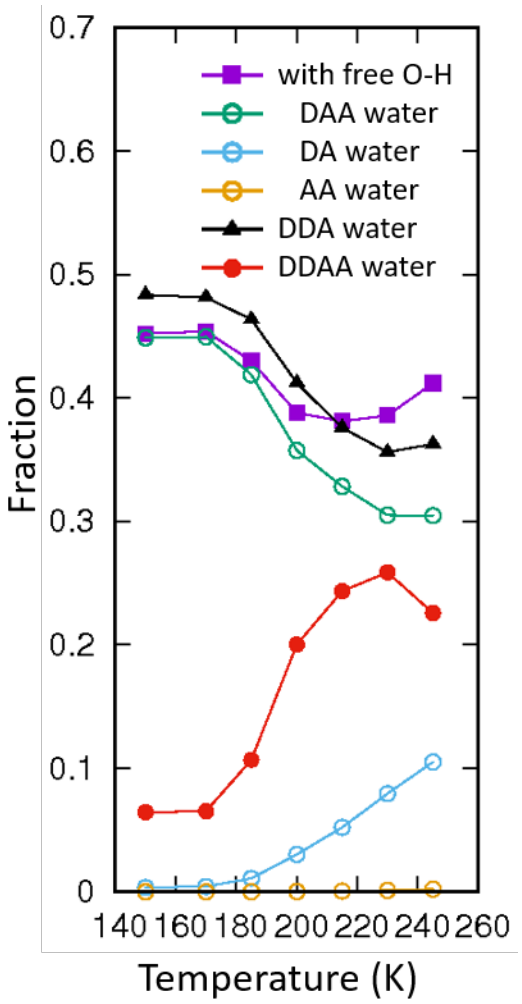

Figure S9. Simulated fractions of different interfacial water species (DAA, DA, AA, DDA, and DDAA water molecules) and total number of water molecules with free O-H groups (DAA + DA + AA) at the topmost monolayer of the ice surface for a H-bond definition of R < 3.5 Å and β < 50° [34]. Error bars are smaller than the size of the symbols.

2.7. SFG Spectra in the C-H Stretch Region

It has been reported that impurities have an effect on the surface structure of ice. [35] In order to confirm the absence of any organic impurities at the surface of ice, we investigated the sum-frequency signal of C-H stretch vibrations in the region 2820-3100 cm^{-1}. As shown in Fig. S10, no prominent C-H contamination was present at the surface, which may imply the negligible effects of the contamination of the SFG spectra at the ice surface.

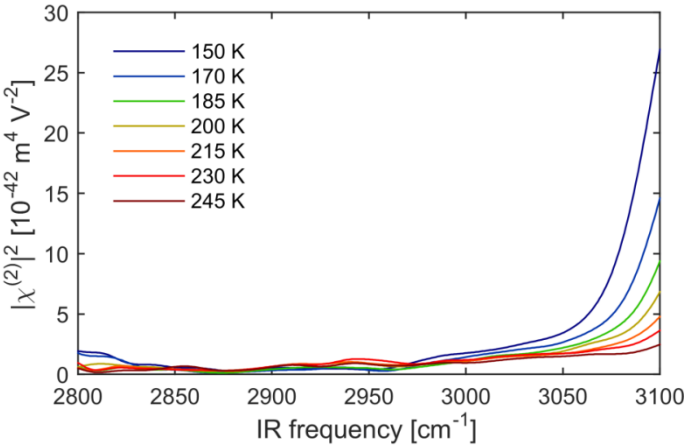

Figure S10. The squared amplitude of the second-order susceptibility ($|\chi^{(2)}|^2$) of the basal surface of ice as a function of temperature.

References:

[1] Y. Nagata and S. Mukamel, J. Am. Chem. Soc. **132**, 6434 (2010).

[2] Y. Nagata, C.-S. Hsieh, T. Hasegawa, J. Voll, E. H. G. Backus, and M. Bonn, J. Phys. Chem. Lett. **4**, 1872 (2013).

[3] P. H. Berens, J. Chem. Phys. **74**, 4872 (1981).

[4] S. D. Ivanov, A. Witt, M. Shiga, and D. Marx, J. Chem. Phys. **132**, 31101 (2010).

[5] T. Hasegawa and Y. Tanimura, J. Phys. Chem. B **115**, 5545 (2011).

[6] G. R. Medders and F. Paesani, J. Am. Chem. Soc. **138**, 3912 (2016).

[7] T. Ohto, K. Usui, T. Hasegawa, M. Bonn, and Y. Nagata, J. Chem. Phys. **143**, 124702 (2015).

[8] Y. Nagata, T. Hasegawa, E. H. G. Backus, K. Usui, S. Yoshimune, T. Ohto, and M. Bonn, Phys. Chem. Chem. Phys. **17**, 23559 (2015).

[9] W. J. Smit, F. Tang, Y. Nagata, M. A. Sanchez, T. Hasegawa, E. H. G. Backus, M. Bonn, and H. J. Bakker, J. Phys. Chem. Lett. **8**, 3656 (2017).

[10] R. Feistel and W. Wagner, J. Phys. Chem. Ref. Data **35**, 1021 (2006).

[11] M. E. Tuckerman, B. J. Berne, and G. J. Martyna, J. Chem. Phys. **97**, 1990 (1992).

[12] H. Yoshida, Phys. Lett. A **150**, 262 (1990).

[13] T. Ishiyama, H. Takahashi, and A. Morita, J. Phys. Chem. Lett. **3**, 3001 (2012).

[14] V. Buch, H. Groenzin, I. Li, M. J. Shultz, and E. Tosatti, Proc. Natl. Acad. Sci. U. S. A. **105**, 5969 (2008).

[15] W. G. Hoover, Phys. Rev. A **31**, 1695 (1985).

[16] I. W. Kuo and C. J. Mundy, Science. **658**, 658 (2004).

[17] A. Luzar and D. Chandler, Nature **379**, 55 (1996).

[18] R. Kumar, J. R. Schmidt, and J. L. Skinner, J. Chem. Phys. **126**, 204107 (2007).

[19] A. Vila Verde, P. G. Bolhuis, and R. K. Campen, J. Phys. Chem. B **116**, 9467 (2012).

[20] I. V. Stiopkin, C. Weeraman, P. A. Pieniazek, F. Y. Shalhout, J. L. Skinner, and A. V. Benderskii, Nature **474**, 192 (2011).

[21] B. M. Auer and J. L. Skinner, J. Chem. Phys. **127**, 104105 (2007).

[22] B. M. Auer and J. L. Skinner, J. Chem. Phys. **128**, 224511 (2008).

[23] E. A. Raymond, T. L. Tarbuck, and G. L. Richmond, J. Phys. Chem. B **106**, 2817 (2002).

[24] E. A. Raymond, T. L. Tarbuck, M. G. Brown, and G. L. Richmond, J. Phys. Chem. B **107**, 546 (2003).

[25] X. Wei, P. Miranda, C. Zhang, and Y. Shen, Phys. Rev. B **66**, 85401 (2002).

[26] X. Wei, P. B. Miranda, and Y. R. Shen, Phys. Rev. Lett. **86**, 1554 (2001).

[27] R. Ramírez, T. López-Ciudad, P. Kumar P, D. Marx, R. Ramírez and, T. López-Ciudad, P. Kumar P, and D. Marx, J. Chem. Phys. **121**, 3973 (2004).

[28] P. Schofield, Phys. Rev. Lett. **4**, 239 (1960).

[29] P. A. Egelstaff, Adv. Phys. **11**, 203 (1962).

[30] T. Joutsuka and K. Ando, J. Chem. Phys. **134**, 204511 (2011).

[31] M. E. Tuckerman and Radu Iftimie, J. Chem. Phys. **122**, 214508 (2005).

[32] R. Ramı, T. L. K. P, D. Marx, and R. Ramı, J. Chem. Phys. **121**, 3973 (2004).

[33] C. P. Lawrence, A. Nakayama, N. Makri, and J. L. Skinner, J. Chem. Phys. **120**, 6621 (2004).

[34] F. Tang, T. Ohto, T. Hasegawa, W. J. Xie, L. Xu, M. Bonn, and Y. Nagata, J. Chem. Theory Comput. submitted.

[35] J. Wettlaufer, Phys. Rev. Lett. **82**, 2516 (1999).